Biointerface Research in Applied Chemistry
Open-Access Journal (ISSN: 2069-5837)

Article
Volume 13, Issue 5, 2023, 438
https://doi.org/10.33263/BRIAC135.438

Removal of Pollutants from Wastewater using Fe-Doped Hydroxyapatite Encapsulated with Alginate

Ayoub Grouli [1,*], Yahya Bachra [1], Fouad Damiri [1], Vikram U Pandit [2], Mohammed Berrada [1]

[1] Laboratory of Analytical and Molecular Chemistry, Department of Chemistry, Faculty of Sciences Ben M'Sick, University Hassan II of Casablanca, Morocco
[2] Departement of Chemistry, Haribhai V. Desai College, Pune-411002, India
* Correspondence: ayoub.grouli-etu@etu.univh2c.ma (A.G.);

Scopus Author ID 57358961400
Received: 2.08.2022; Accepted: 20.09.2022; Published: 19.12.2022

Abstract: Alginate is a natural biopolymer that can be processed into various usable forms, such as beads or membranes, for its application in water treatment technology. The present study aimed to synthesize beads of alginate biocomposites encapsulated in magnetic nano-hydroxyapatite (m@HA-Alg), magnetic bentonite (m@Bent-Alg), and magnetic attapulgite (m@Att-HA) using the co-precipitation method as well as employing them as adsorbents for the removal of Congo red (CR) dye by adsorption. The synthesized magnetic nano-hydroxyapatite (m@HA-Alg) exhibited a better CR sorption capacity (SC) of 76.14 mg/g than the individual components and biocomposites. Different instrumental techniques such as Fourier transform infrared spectroscopy (FTIR), X-ray diffraction (XRD), scanning electron microscopy (SEM), and thermal gravimetric analysis (TGA) were used to characterize these synthesized materials and investigate their intrinsic properties. The biocomposites' reusability was achieved using the NaOH eluent and sorption product.

Keywords: alginate; biocomposites; magnetic; diffusion; sorption.

1. Introduction

Water is an essential resource for all creations of life, and water quality is closely linked to human survival and health, as well as to the running of industry and agriculture. In the last decades, many dyes have been discharged into rivers and aquatic mediums without any preliminary treatment [1–4]. Absorption of dyes discharged into the water bodies adversely impacts aquatic life and poses a threat to public health [5]. Of all the organic compounds in the water, the elimination of dyes is the most challenging. Congo Red (CR) is an anionic dye with a chemical formula $C_{32}H_{22}N_6Na_2O_6S_2$ and an IUPAC name of the sodium salt of benzidinediazo-bis-1-naphthylamine-4-sulfonic acid [6]. CR is not fully biodegradable and can cause health issues such as dizziness, emesis, defecation, and diarrhea [7]. This dye is also used in various industries, such as the textile industry, due to its high attractiveness with cellulose fibers, papermaking, cosmetics, pharmaceutical products, and plastic.

On the other hand, these dyes are water-soluble, resistant to light and chemicals, and are not easily removed from wastewater. Discharging colored wastewater leads to ecosystem toxicity and bioaccumulation of these dyes in the living bodies of marine organisms [8–10]. In addition, the presence of dyes in the effluent prevents sunlight from penetrating the water and reduces the light's intensity, inhibiting the photosynthetic process on the water surface [11].

Nowadays, researchers have developed different methods to reduce contaminants and dye concentration from wastewater. These methods include biological treatment such as fungal reactors, bioremediation, and microbial degradation [12, 13]. Chemical treatment includes coagulation, electroflotation, electrokinetic coagulation, photocatalytic oxidation, and irradiation [14–17]. Otherwise, physical treatment encompasses filtration and adsorption [18–21]. Among these several methods for dye elimination from wastewater, adsorbents have been extensively studied up to the present time. They have been investigated for their intrinsic properties, simple design, easy process, cost-effectiveness, and high-efficiency rate. Meanwhile, recovering adsorbents from wastewater is still difficult to manage. Scientists have proposed a filtration method that requires specific diameters of filter, which was partially not efficient despite the high cost of the process [22].

Hydroxyapatite (HA) has attracted scientific interest as a functional inorganic material because of its unique intrinsic properties in medicine as a bone replacement material that promotes cell proliferation and accelerates the healing process [23]. The main structure of HA is $Ca_{10}(PO_4)_6(OH)_2$, and it demonstrates excellent biocompatibility and bioactivity. HA can easily be prepared from bovine-rich sources (dromedary bone, bovine bone, eggshells, etc.). In order to fulfill the criterion, eggshell was considered an efficient source of calcium, as it was noted that 95% of eggshell waste contains calcium in $CaCO_3$ form. Furthermore, modifying the HA surface with a variety of molecules could enhance its surface properties and make it a good alternative adsorbent for eliminating CR dye from an aqueous medium [24].

Owing to their phenomenal potential for application in wastewater treatment, magnetic hydroxyapatite (m@HA) nanoparticles have also been gaining significant attention. Magnetite (Fe_3O_4) nanoparticles are the most widely used magnetic materials due to their attainable superparamagnetic properties at ambient conditions, biocompatibility, and high magnetic moment resulting from the unique structure of these nanoparticles. As a result of these notable properties and cost-effectiveness of these materials, they are extensively applied in different fields such as pharmaceutical industries, wastewater treatment, etc. [25]. Although magnetite is chemically inert, the combined superparamagnetic and high magnetic susceptibility make their manipulation under an external magnetic field simple and efficient [26]. However, magnetite nanoparticles have been studied at the laboratory for adsorption studies to remove various types of contaminants, such as dyes, heavy metals, etc.

Alginates are naturally-occurring linear block copolymers comprising 1,4-linked β-D-mannuronic acid (M) and a-L-guluronic acid (G). The physical properties of the alginate products are majorly influenced by the contents of M and G present in the alginates, which depend on the different species of seaweed used for their extraction. Sodium alginate (SA) is one such polymer found in brown algae, and it is known for forming good fibers and strong membranes in the solid state due to its linear structure and high molecular weight. It is also known for its non-toxicity and biocompatibility with many cells. The presence of excessive carboxyl and hydroxyl groups along its polymer structure enables its application as an adsorbent with better adsorption efficiency for removing heavy metals from aqueous media. It is generally functionalized with other materials to overcome its drawbacks and enhance its adsorption efficiency [27–30].

Biocomposites were considered efficient adsorbents to remove contaminants from wastewater. Bentonite demonstrated good removal behavior for most common industrial pollutants due to its surface being negatively charged.

The present work aimed to study the CR dye's removal rate using m@HA-Alg biocomposite from contaminant wastewater. The intrinsic properties of the aforementioned nanomaterial biocomposite were fully examined by SEM, TGA, XRD, and FTIR analysis techniques. Furthermore, the influence of different parameters on the CR dye sorption was also evaluated. The biocomposite demonstrated easy separation from the solution using a magnet. Adsorption, considered an effective technique for sequestering heavy metals and removing polluting dyes, has been proposed as an excellent way to treat wastewater with dyes and other coloring agents.

2. Materials and Methods

Congo Red (CR) was purchased from Sigma Aldrich. Eggshell waste was locally collected. Phosphoric Acid (H_3PO_4) and iron oxide II ($FeCl_2{\cdot}4H_2O$) and iron oxide III ($FeCl_3{\cdot}6H_2O$), Ethylene Diamine Tetra Acetic acid EDTA $[CH_2N(CH_2CO_2H)_2]_2$ (Sigma Aldrich), and all reagents have been used as received, without any additional purification. Sodium alginate and sodium bentonite, and attapulgite were employed as received.

2.1. Preparation of egg-HA.

Before extraction of CaO from eggshell waste, some steps were adopted to eliminate the presence of contaminant and organic components. The eggshell waste was washed with chloride acid and water and then dried for a week under solar radiation. The powder was placed in a furnace at 1000°C. The chemical reactions involved were as follows:

$$CaCO_3 \xrightarrow{1000^{\circ}C} CaO + CO_3 \ (\mathbf{1})$$

$$CaO + H_20 \rightarrow Ca(OH)_2 \quad (\mathbf{2})$$

$$10Ca(OH)_2 + 6H_3PO_4 \rightarrow Ca_{10}(PO_4)_6(OH)_2 + 18H_2O \ (\mathbf{3})$$

As can be seen from Figure 1, eggshell powder (CaO) was used as a precursor to prepare a 1.0 M calcium hydroxide solution, to which 0.6 M phosphoric acid was added as a source of phosphate ions under continuous stirring using a magnetic stirrer at 80°C. A milky white solution was obtained, and ammonium hydroxide (NH_4OH) solution was gradually added to keep the pH over 10 and prevent the formation of calcium-deficient apatite [31].

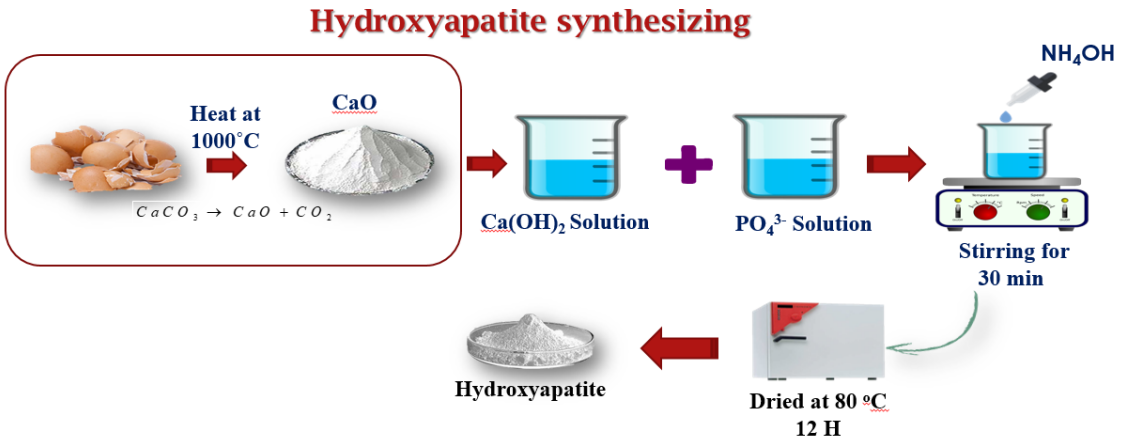

Figure 1. Schematic representation of hydroxyapatite preparation.

2.2. Preparation of magnetite Fe_3O_4 nanoparticles.

According to our previous work, the iron oxide nanoparticles (Fe_3O_4) were successfully prepared by mixing 0.015mol of $FeCl_2 \cdot 4H_2O$, and 0.03mol of $FeCl_3 \cdot 6H_2O$ in 100ml of water and continue stirring for 1h. During the reaction, ammonium hydroxide (NH_4OH) was added dropwise to maintain the pH above 9, followed by adding 50 mL of EDTA to stabilize the magnetite [32, 33]. Finally, the dark solution of magnetite was formed. Iron oxide was recovered by using a strong magnetic field and washed several times with DI water.

2.3. Preparation of biocomposites.

Around 2 g of magnetic hydroxyapatite (m@HA) and magnetic bentonite (m@Bent), and magnetic attapulgite (m@Att) powder were first sonicated for 2 hours, then mixed with 100 ml of 2% sodium alginate solution and stirred vigorously for 3 hours to obtain homogeneous solutions. Then the above solutions were poured into a 4% calcium chloride solution to obtain spherical particles of m@HA-Alg, m@Bent-Alg, and m@Att-Alg. The obtained spherical particles were immersed in calcium chloride solution overnight for complete cross-linking with Ca^{2+} ions. The resulting m@HA-Alg biocomposite was then transferred to an autoclave and heated to 140 °C for 24 hours. The hydrothermally treated magnetic biocomposites were then washed with distilled water to a neutral pH and dried in a hot air oven at 90 °C for 12 hours. Meanwhile, the dried m@HA-Alg, m@Bent-Alg, and m@Att-Alg biocomposites were used for Congo red sorption studies.

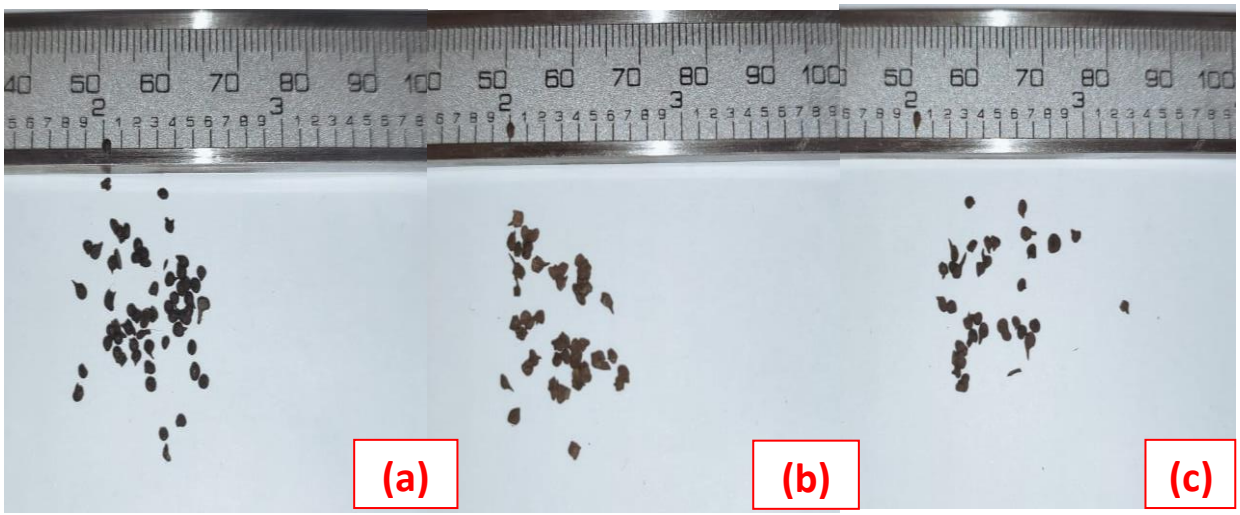

Figure 2. Biocomposites beads of: (a)m@HA-Alg, (b) m@Bent-Alg, (c) m@Att-Alg.

2.4. Characterization.

2.4.1. Fourier Transform Infrared Spectroscopy (FTIR).

Fourier transform infrared spectroscopy (FTIR) spectra of HA, m@HAP-Alg, and all adsorbents were established with the preparation of KBr pellets on a Bruker Tensor-27 spectrophotometer from Bruker Corporation (Germany). The infrared transmittance method was used, and all spectra averaged 32 scans from 4000 to 400 cm^{-1} at a resolution of 4 cm^{-1}.

2.4.2. Thermogravimetric Analysis (TGA).

Thermogravimetric analysis (TGA) was conducted on a Setsys Evolution 16/18 TGA/DTA instrument (SETARAM). The samples were subjected to a heating rate of 15°C/min in a temperature range of 40 to 900°C.

2.4.3. X-Ray Diffraction Analysis (XRD).

The X-ray diffraction pattern (XRD) of HA was investigated with a Bruker D8-Advance X-ray powder diffractometer (Germany) using nickel-filtered Cu-Kα radiation (λ = 1.54056° A) with a potential of 40 kV and an intensity of 100 mA. The diffused radiation has been detected at the angle range of 10-80° (2θ), with a stepping point of 0.01° (2θ).

2.4.4. Scanning Electron Microscopy (SEM).

Morphological analysis of HA and adsorbents was realized by scanning electron microscopy (SEM) using a MiniSEM Hirox model SH-4000M.

2.5. Dyes pollutants removal experiment on HAP.

Three biocomposites were used for the removal of Congo red dye, and the residual concentration was measured by a spectrophotometer (Shimadzu, Japan) at 500 nm. The equilibrium adsorption capacity, Qe (mg/g), and removal efficiency R (%), of CR onto adsorbents were calculated using formulas (a) and (b), respectively:

$$Q_e = \frac{(C_0 - C_e)V}{m} \quad \textbf{(a)} \qquad R(\%) = \frac{C_0 - C_e}{C_0} \times 100 \quad (\textbf{b})$$

where C_o and C_e are the initial and equilibrium CR concentrations (mg/L), V is the volume of the solution, and m is the mass of the egg-HA sample (g) for the adsorption.

3. Results and Discussion

3.1. Characterization of egg-HA.

The FTIR pattern of calcined eggshells was investigated as a first-step procedure for the chemical identification of eggshell-derived calcium oxide. Figure 3 shows an FTIR pattern of eggshell-derived calcium oxide. The corresponding peaks at 1455, 910, and 720 cm^{-1} belong to the carbonate group in $CaCO_3$, which is normally considered the principal constituent of eggshells, as reported by Ravindran et al. [34, 35]. Furthermore, during the experiment, it was easy to sorb gas due to the highly porous structure of calcium oxide. The minor frequency bands at 2910 and 2520 cm^{-1} were the most prominent observed and were assigned to the combining modes of the various CO_2 molecules. In addition, the peak at 3655 cm^{-1} was attributed to a hydroxyl group. Therefore, the vibration between O-H was detected due to moisture absorption [36]. Three frequency bands intrinsic to the CaO structure were evident. The broad bands at 1455 and 1020 cm^{-1} were attributed to the C-O stretching mode concerning CO2 adsorbed on the CaO surface. Thus, it remains important to mention that there was no significant change in the result of the FTIR spectra. Therefore, a preliminary experiment of the FTIR spectrum may indicate that calcium oxide was successfully obtained from eggshells.

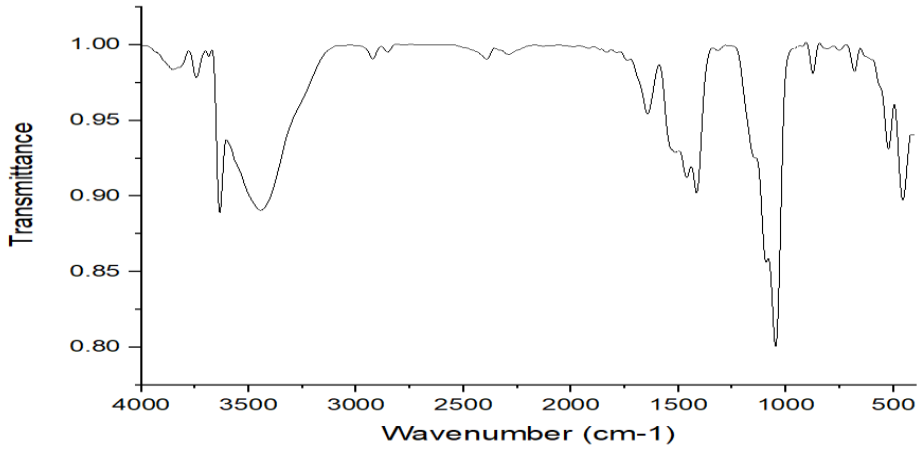

Figure 3. IR spectrum of Calcium Oxide CaO.

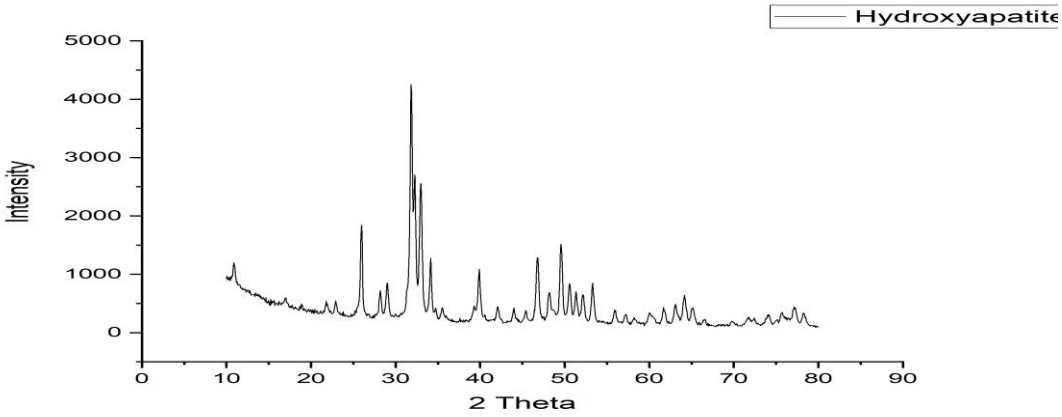

Figure 4. XRD pattern of hydroxyapatite prepared calcium oxide at 900°C.

The preliminary experiments could confirm the successful synthesis of hydroxyapatite by wet co-precipitation. Eggshell waste can be used effectively as a substitute for calcium sources. After the preparation of calcium oxide, the preliminary experiment as a source of HA precursor was then studied. The obtained results showed that eggshell-derived calcium oxide exhibited excellent performance in forming HA. Figure 4 shows the XRD pattern of the as-synthesized hydroxyapatite powder. It was observed that peaks with the highest intensities peak at 2θ equaling 25.85, 31.17, and 32.90, were attributed as HA. According to Ebenezer *et al.*, the following miller indices (hkl) for the above-mentioned 2θ were (002), (112), and (300). A peak corresponding to calcium-deficient apatite $Ca_3(PO_4)_2$ at 32.17 was also presented. The following results might be seen in the removal efficiency of RC dye pollutants.

To determine the rate of humidity and thermal behavior of HAP, the sample was heated from ambient temperature to 900°C. Figure 5 shows three regions from ambient temperature to 500 °C during TGA. No significant weight loss was observed at 500 °C. A slight decomposition of egg-HA was observed due to the elimination of carbon dioxide molecules, and these results can confirm that the egg-HA is stable under the temperature range from ambient to 900 °C.

The hydroxyapatite and alginate magnetite (m@HA-Alg) biocomposite were successfully prepared. As can be seen in Figure 4, egg-HA was distributed into Alg/Mag with good uniformity. Figure 6 Neat adsorbents were also used for comparison. Based on the structural properties of egg-HA, the absorption bands observed around 510 cm^{-1} and 1035 cm^{-1} were assigned to phosphate group vibration.

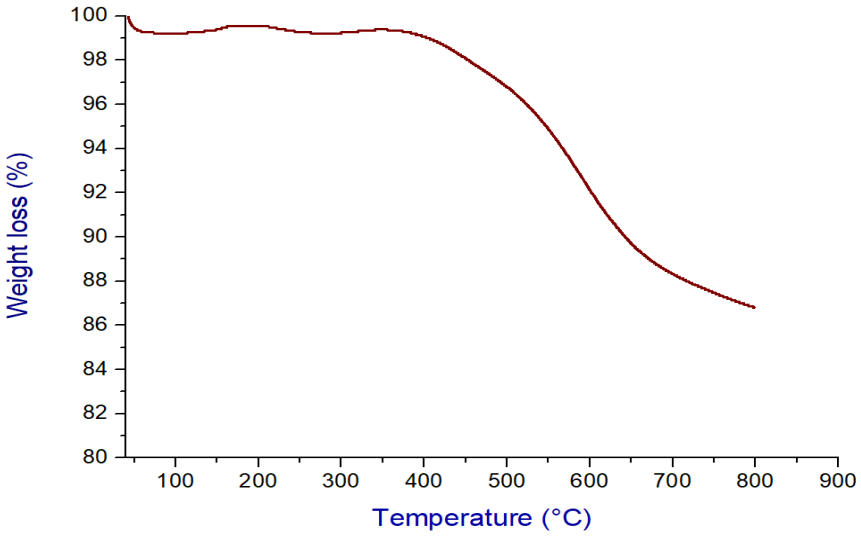

Figure 5. TGA curve of Hydroxyapatite from eggshell-based material.

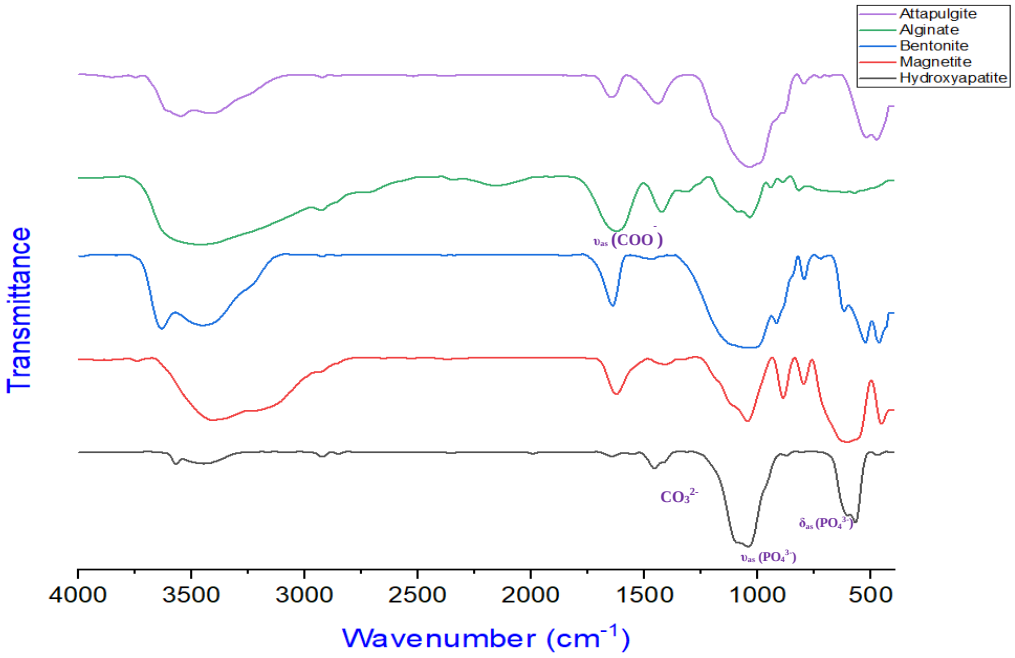

Figure 6. FTIR Spectra of Hydroxyapatite and adsorbent's clays.

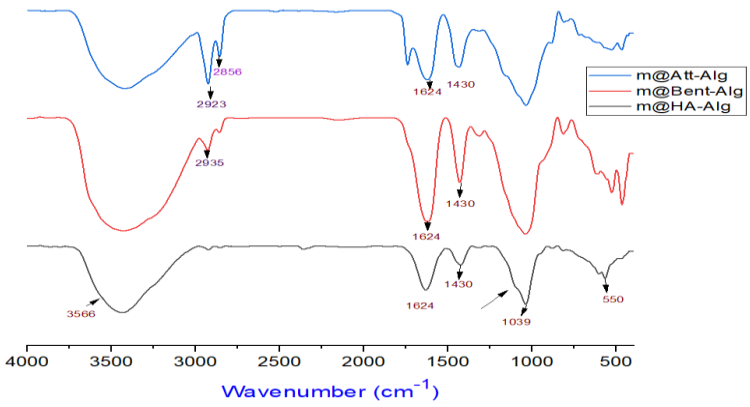

Figure 7. FTIR Spectra the Biocomposite adsorbent.

In addition, absorption characteristic peaks at the wavenumber of 3566 cm^{-1} and 591 cm^{-1} were assigned to hydroxide OH- stretching vibrations. Figure 7 shows that for all biocomposites, two characteristic bands at 1624 and 1430 cm^{-1} are assigned to -COO groups of alginate, indicating the successful encapsulation of hydroxyapatite and alginate. Furthermore, two characteristic bands of magnetite also appeared in all biocomposites, thus indicating the presence of controllable magnetic particles.

3.2. UV Scanning Electron Microscopy (SEM) observation.

The surface morphology of the adsorbents was investigated using SEM. Figure 8 shows the surface morphology of pure HA microspheres obtained from eggshells (A), Magnetite (B), and biocomposites (Figure 7 A-D). Figure 7A of Pristine HA demonstrates a porous structure of ~ 15-30 µm and a rough surface. Figure 7C exhibits regular round structures and agglomerates of m@HA-Alg biocomposites [37]. Thus, the successful preparation of adsorbent with homogenous, spherical particles with enhanced surface properties can be confirmed, along with the presence of some cavities formed. Thereby, the effect is clear when HA is replaced with sodium bentonite. Figure 7D shows the continuous structure with enhanced surface roughness due to the improved interconnectivity between the compounds. However, the porosity of the biocomposite m@HA-Alg enhanced dye uptake in CR and heavy metals [38, 39].

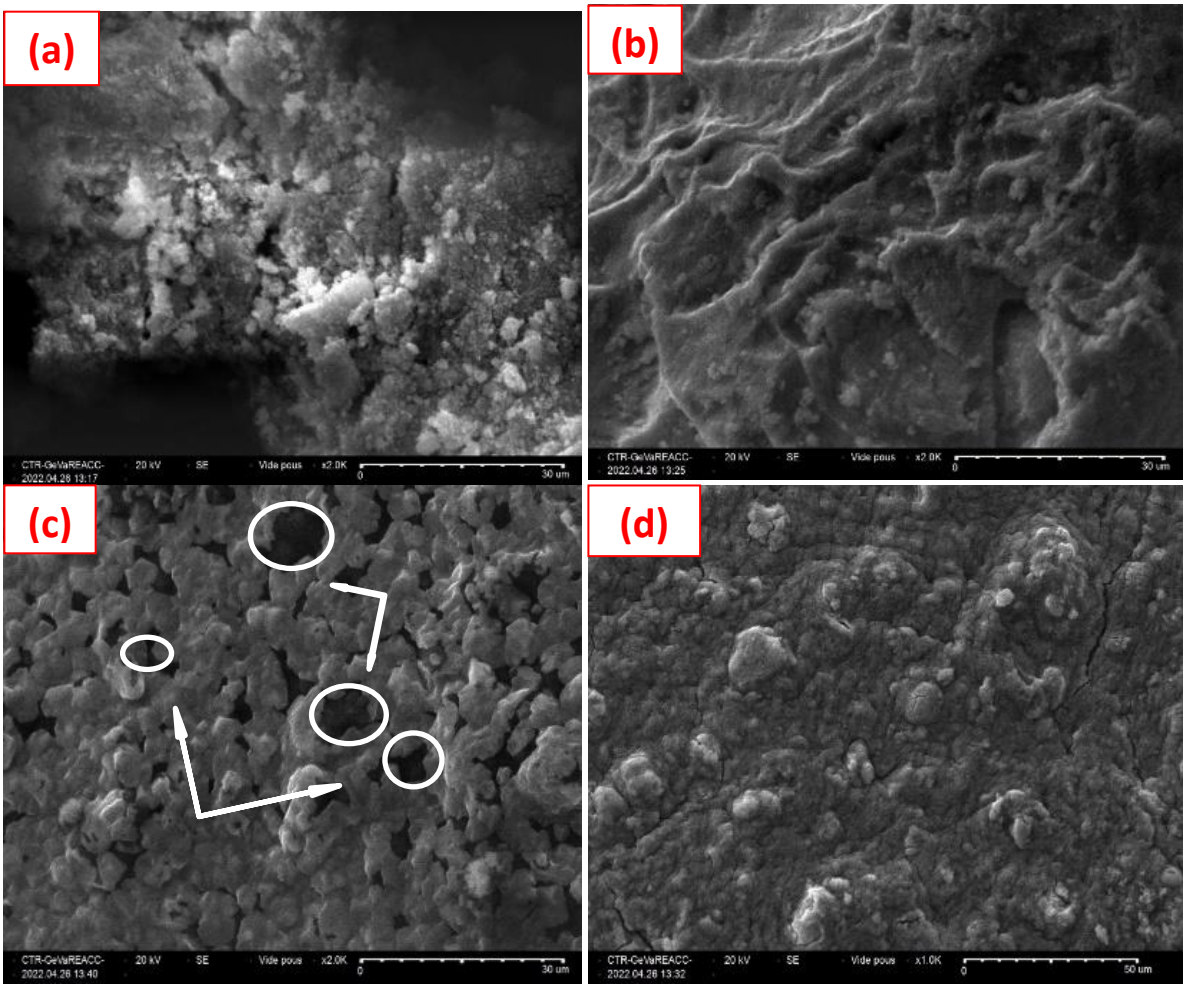

Figure 8. SEM images of (a) eggshell Hydroxyapatite, (b) Magnetite,(c) m@HA-Alg, (d) m@Bent-Alg.

3.3. Adsorption experiments.

3.3.1. Effect of adsorbent amount.

It can be seen in Figures 9 and 10 that HAP biocomposite has the highest removal rate (82%) at the equilibrium when the mass reaches 0.25 g. The bentonite biocomposite shows similar results, which can be explained by the negatively charged surface of the biocomposite interacting with the positively charged group of Congo red [40, 41]. On the other hand, the attapulgite biocomposite shows a lower removal rate due to its surface properties.

Figure 9. Discoloration approach of RC Congo solution by m@HA-Alg biocomposite.

Figure 11 shows that the adsorption capacity of each biocomposite technically decreases with an increase in the adsorbent amount. It was reported in recent similar studies that this phenomenon is due to the saturation of adsorption sites and the non-availability of the surface area.

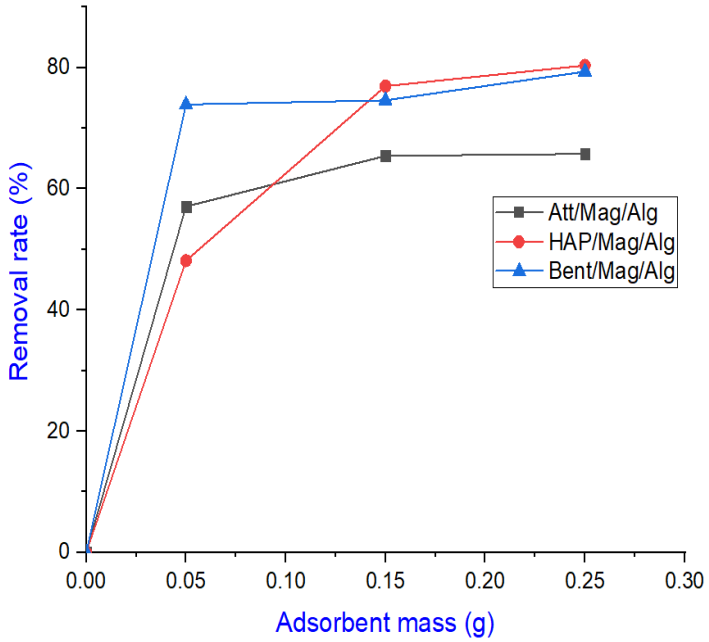

Figure 10. Effect of adsorbent mass on RC removal.

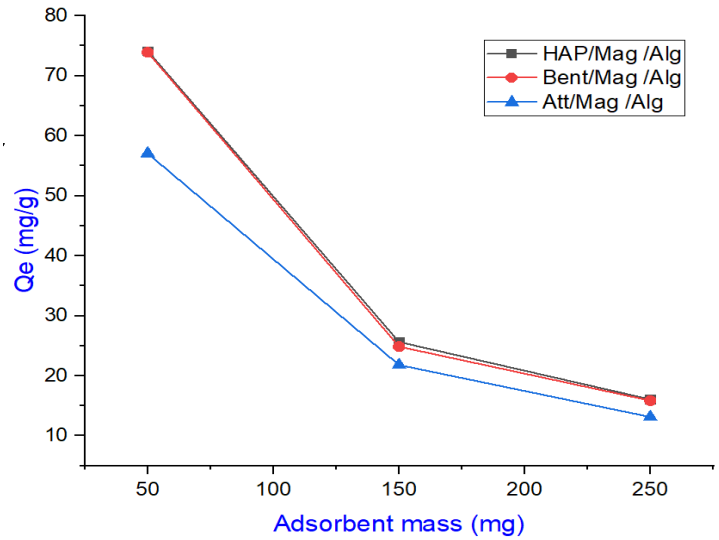

Figure 11. Effect of adsorbent mass on RC adsorption by HAP/Mag/Alg, Att/Mag/Alg, Bent/Mag/Alg (adsorption conditions: initial RC concentration 50 mg/L, solution volume= 50 ml, temperature 25°C, contact time= 3h).

3.3.2. Effect of initial pH.

The effect of pH on the adsorption of CR was evaluated by varying pH to control the adsorption mechanism by modifying the surface charges of the adsorbent as well as CR. It has been reported in previous studies that hydroxyapatite demonstrates significant adsorption capacity against CR in an acidic medium [42]. The results illustrated in Figure 12 indicate that the adsorption capacity of adsorbent against CR is lower in an alkaline solution, which could possibly be explained by the existence of negatively charged ions on the surface. Therefore, the removal of CR by adsorption using hydroxyapatite is unfavorable in an alkaline medium. Otherwise, a notable adsorption capacity is demonstrated in an acidic medium.

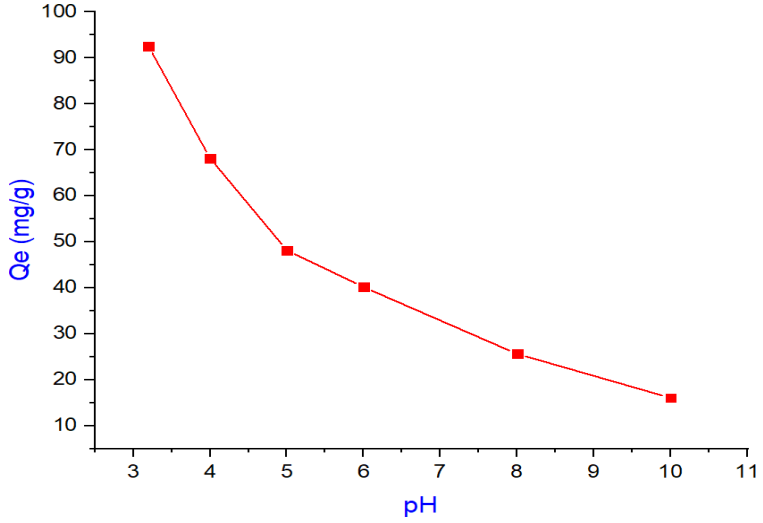

Figure 12. Effect of initial pH on m@HA-Alg removal of CR solution.

The observed mechanism of the high attraction of the dye is possibly due to an electrostatic interaction between the surface of the natural adsorbent (hydroxyl and phosphate groups) and the CR molecules (sulfonic groups) [43]. These observations are consistent with the pHpzc value of 8 of the adsorbent. Since the maximum adsorption was noticed at pH 5, the same value was chosen as the optimal pH for further adsorption tests.

4. Conclusions

A wet chemical precipitation method was adopted in the present study to synthesize hydroxyapatite from eggshell waste as a source of calcium oxide. Further, nanomaterials based on eggshell hydroxyapatite and magnetite encapsulated with sodium alginate were developed as well as employed as an adsorbent for the removal of dye pollutants, and their performance was compared with that of bentonite biocomposite. In the present study, the application of hydroxyapatite as an adsorbent was evaluated for the reduction of congo red dye concentration in a wastewater sample. Its structural and chemical properties as well as the thermal stability were analyzed using XRD, FTIR, and TGA, respectively. The influence of different parameters such as pH, dye concentration, and adsorbent dose on the adsorption of congo red was studied. From the results obtained, it was observed that the point of zero charges (pHpzc) for the adsorbent was 8, and the maximum adsorption capacity of the hydroxyapatite for congo red was achieved after 180 minutes at pH 5.

Funding

This research received no external funding.

Acknowledgments

Declared none.

Conflicts of Interest

The authors declare no conflict of interest.

References

1. Slama, H.B.; Chenari Bouket, A.; Pourhassan, Z.; Alenezi, F.N.; Silini, A.; Cherif-Silini, H.; Oszako, T.; Luptakova, L.; Golińska, P.; Belbahri, L. Diversity of Synthetic Dyes from Textile Industries, Discharge Impacts and Treatment Methods. *Appl. Sci.* **2021**, *11*, 6255, https://doi.org/10.3390/app11146255.
2. Pang, Y.L.; Abdullah, A.Z. Current Status of Textile Industry Wastewater Management and Research Progress in Malaysia: A Review. *CLEAN - Soil Air Water* **2013**, *41*, 751–764, https://doi.org/10.1002/clen.201000318.
3. Al-Tohamy, R.; Ali, S.S.; Li, F.; Okasha, K.M.; Mahmoud, Y.A.-G.; Elsamahy, T.; Jiao, H.; Fu, Y.; Sun, J. A Critical Review on the Treatment of Dye-Containing Wastewater: Ecotoxicological and Health Concerns of Textile Dyes and Possible Remediation Approaches for Environmental Safety. *Ecotoxicol. Environ. Saf.* **2022**, *231*, 113160, https://doi.org/10.1016/j.ecoenv.2021.113160.
4. Al-Ansari, M.M.; Li, Z.; Masood, A.; Rajaselvam, J. Decolourization of Azo Dye Using a Batch Bioreactor by an Indigenous Bacterium Enterobacter Aerogenes ES014 from the Waste Water Dye Effluent and Toxicity Analysis. *Environ. Res.* **2022**, *205*, 112189, https://doi.org/10.1016/j.envres.2021.112189.
5. Zheng, Y.; Zhang, J. Experimental Study on the Adsorption of Dissolved Heavy Metals by Nano-Hydroxyapatite. *Water Sci. Technol.* **2020**, *82*, 1825–1832, https://doi.org/10.2166/wst.2020.465.
6. Himanshu Patel, R.T. Vashi Removal of Congo Red Dye from Its Aqueous Solution Using Natural Coagulants. *J. Saudi Chem. Soc.* **2012**, *16*, 131–136, https://doi.org/10.1016/j.jscs.2010.12.003.
7. Sathiyavimal, S.; Vasantharaj, S.; Shanmugavel, M.; Manikandan, E.; Nguyen-Tri, P.; Brindhadevi, K.; Pugazhendhi, A. Facile Synthesis and Characterization of Hydroxyapatite from Fish Bones: Photocatalytic Degradation of Industrial Dyes (Crystal Violet and Congo Red). *Prog. Org. Coat.* **2020**, *148*, 105890, https://doi.org/10.1016/j.porgcoat.2020.105890.
8. Goud, B.S.; Cha, H.L.; Koyyada, G.; Kim, J.H. Augmented Biodegradation of Textile Azo Dye Effluents by Plant Endophytes: A Sustainable, Eco-Friendly Alternative. *Curr. Microbiol.* **2020**, *77*, 3240–3255, https://doi.org/10.1007/s00284-020-02202-0.

9. Mustafa, S.; Bhatti, H.N.; Maqbool, M.; Iqbal, M. Microalgae Biosorption, Bioaccumulation and Biodegradation Efficiency for the Remediation of Wastewater and Carbon Dioxide Mitigation: Prospects, Challenges and Opportunities. *J. Water Process Eng.* **2021**, *41*, 102009, https://doi.org/10.1016/j.jwpe.2021.102009.
10. Oke, N.; Mohan, S. Development of Nanoporous Textile Sludge Based Adsorbent for the Dye Removal from Industrial Textile Effluent. *J. Hazard. Mater.* **2022**, *422*, 126864, https://doi.org/10.1016/j.jhazmat.2021.126864.
11. Esmaeili, H.; Foroutan, R. Adsorptive Behavior of Methylene Blue onto Sawdust of Sour Lemon, Date Palm, and Eucalyptus as Agricultural Wastes. *J. Dispers. Sci. Technol.* **2019**, *40*, 990–999, https://doi.org/10.1080/01932691.2018.1489828.
12. Hai, F.I.; Yamamoto, K.; Nakajima, F.; Fukushi, K. Factors Governing Performance of Continuous Fungal Reactor during Non-Sterile Operation – The Case of a Membrane Bioreactor Treating Textile Wastewater. *Chemosphere* **2009**, *74*, 810–817, https://doi.org/10.1016/j.chemosphere.2008.10.025.
13. Ajaz, M.; Shakeel, S.; Rehman, A. Microbial Use for Azo Dye Degradation—a Strategy for Dye Bioremediation. *Int. Microbiol.* **2020**, *23*, 149–159, https://doi.org/10.1007/s10123-019-00103-2.
14. Szyguła, A.; Guibal, E.; Ruiz, M.; Sastre, A.M. The Removal of Sulphonated Azo-Dyes by Coagulation with Chitosan. *Colloids Surf. A: Physicochem. Eng. Asp.* **2008**, *330*, 219–226, https://doi.org/10.1016/j.colsurfa.2008.08.001.
15. Said, B.; M'rabet, S.; Hsissou, R.; Harfi, A.E. Synthesis of New Low-Cost Organic Ultrafiltration Membrane Made from Polysulfone/Polyetherimide Blends and Its Application for Soluble Azoic Dyes Removal. *J. Mater. Res. Technol.* **2020**, *9*, 4763–4772, https://doi.org/10.1016/j.jmrt.2020.02.102.
16. So, C.M.; Cheng, M.Y.; Yu, J.C.; Wong, P.K. Degradation of Azo Dye Procion Red MX-5B by Photocatalytic Oxidation. *Chemosphere* **2002**, *46*, 905–912, https://doi.org/10.1016/S0045-6535(01)00153-9.
17. Ji, P.; Zhang, J.; Chen, F.; Anpo, M. Study of Adsorption and Degradation of Acid Orange 7 on the Surface of CeO_2 under Visible Light Irradiation. *Appl. Catal. B Environ.* **2009**, *85*, 148–154, https://doi.org/10.1016/j.apcatb.2008.07.004.
18. García, E.R.; Medina, R.L.; Lozano, M.M.; Hernández Pérez, I.; Valero, M.J.; Franco, A.M.M. Adsorption of Azo-Dye Orange II from Aqueous Solutions Using a Metal-Organic Framework Material: Iron-Benzenetricarboxylate. *Materials* **2014**, *7*, 8037–8057, https://doi.org/10.3390/ma7128037.
19. Moughaoui, F.; Ouaket, A.; Laaraibi, A.; Hamdouch, S.; Anbaoui, Z.; Abourriche, A.; Berrada, M. A Novel Approach for Producing Low Cost and Highly Efficient Activated Carbon for Removing Cationic Dyes. *Mediterr. J. Chem.* **2019**, *8*, 74–83, http://dx.doi.org/10.13171/10.13171/mjc8219040103fm.
20. Malek, N.N.A.; Jawad, A.H.; Abdulhameed, A.S.; Ismail, K.; Hameed, B.H. New Magnetic Schiff's Base-Chitosan-Glyoxal/Fly Ash/Fe_3O_4 Biocomposite for the Removal of Anionic Azo Dye: An Optimized Process. *Int. J. Biol. Macromol.* **2020**, *146*, 530–539, https://doi.org/10.1016/j.ijbiomac.2020.01.020.
21. Abramian, L.; El-Rassy, H. Adsorption Kinetics and Thermodynamics of Azo-Dye Orange II onto Highly Porous Titania Aerogel. *Chem. Eng. J.* **2009**, *150*, 403–410, https://doi.org/10.1016/j.cej.2009.01.019.
22. Hoslett, J.; Massara, T.M.; Malamis, S. et al. Surface Water Filtration Using Granular Media and Membranes: A Review. *Sci. Total Environ.* **2018**, *639*, 1268–1282, https://doi.org/10.1016/j.scitotenv.2018.05.247.
23. Christy, P.N.; Basha, S.K.; Kumari, V.S.; Bashir, A.K.H.; Maaza, M.; Kaviyarasu, K.; Arasu, M.V.; Al-Dhabi, N.A.; Ignacimuthu, S. Biopolymeric Nanocomposite Scaffolds for Bone Tissue Engineering Applications – A Review. *J. Drug Deliv. Sci. Technol.* **2020**, *55*, 101452, https://doi.org/10.1016/j.jddst.2019.101452.
24. Wang, H.; Yan, K.; Chen, J. Preparation of Hydroxyapatite Microspheres by Hydrothermal Self-Assembly of Marine Shell for Effective Adsorption of Congo Red. *Mater. Lett.* **2021**, *304*, 130573, https://doi.org/10.1016/j.matlet.2021.130573.
25. Bachra, Y.; Grouli, A.; Damiri, F.; Talbi, M.; Berrada, M. A Novel Superabsorbent Polymer from Crosslinked Carboxymethyl Tragacanth Gum with Glutaraldehyde: Synthesis, Characterization, and Swelling Properties. *Int. J. Biomater.* **2021**, *2021*, 5008833, https://doi.org/10.1155/2021/5008833.
26. Falciglia, P.P.; Gagliano, E.; Scandura, P. et al. Physico-Magnetic Properties and Dynamics of Magnetite (Fe_3O_4) Nanoparticles (MNPs) under the Effect of Permanent Magnetic Fields in Contaminated Water Treatment Applications. *Sep. Purif. Technol.* **2022**, *296*, 121342, https://doi.org/10.1016/j.seppur.2022.121342.

27. Sutirman, Z.A.; Sanagi, M.M.; Wan Aini, W.I. Alginate-Based Adsorbents for Removal of Metal Ions and Radionuclides from Aqueous Solutions: A Review. *Int. J. Biol. Macromol.* **2021**, *174*, 216–228, https://doi.org/10.1016/j.ijbiomac.2021.01.150.
28. Nabizad, M.; Dadvand Koohi, A.; Erfanipour, Z. Removal of Cefixime Using Heterogeneous Fenton Catalysts: Alginate/Magnetite Hydroxyapatite Nanocomposite. *J. Water Environ. Nanotechnol.* **2022**, *7*, 14-30, https://doi.org/10.22090/jwent.2022.01.002.
29. Guesmi, Y.; Agougui, H.; Lafi, R.; Jabli, M.; Hafiane, A. Synthesis of Hydroxyapatite-Sodium Alginate via a Co-Precipitation Technique for Efficient Adsorption of Methylene Blue Dye. *J. Mol. Liq.* **2018**, *249*, 912–920, https://doi.org/10.1016/j.molliq.2017.11.113.
30. Bachra, Y.; Grouli, A.; Damiri, F.; Bennamara, A.; Berrada, M. A New Approach for Assessing the Absorption of Disposable Baby Diapers and Superabsorbent Polymers: A Comparative Study. *Results in Mater.* **2020**, *8*, 100156, https://doi.org/10.1016/j.rinma.2020.100156.
31. Ummartyotin, S.; Tangnorawich, B. Utilization of Eggshell Waste as Raw Material for Synthesis of Hydroxyapatite. *Colloid Polym. Sci.* **2015**, *293*, 2477–2483, https://doi.org/10.1007/s00396-015-3646-0.
32. Fouad, D.; Bachra, Y.; Ayoub, G.; Ouaket, A.; Bennamara, A.; Knouzi, N.; Berrada, M. A Novel Drug Delivery System Based on Nanoparticles of Magnetite Fe_3O_4 Embedded in an Auto Cross-Linked Chitosan. *In*: *Berrada, M (Ed.), Chitin and Chitosan - Physicochemical Properties and Industrial Applications*, IntechOpen, **2020**, https://doi.org/10.5772/intechopen.91553.
33. Jafari Eskandari, M.; Hasanzadeh, I. Size-Controlled Synthesis of Fe_3O_4 Magnetic Nanoparticles via an Alternating Magnetic Field and Ultrasonic-Assisted Chemical Co-Precipitation. *Mater. Sci. Eng. B* **2021**, *266*, 115050, https://doi.org/10.1016/j.mseb.2021.115050.
34. Goh, K.W.; Wong, Y.H.; Ramesh, S.; Chandran, H.; Krishnasamy, S.; Ramesh, S.; Sidhu, A.; Teng, W.D. Effect of PH on the Properties of Eggshell-Derived Hydroxyapatite Bioceramic Synthesized by Wet Chemical Method Assisted by Microwave Irradiation. *Ceram. Int.* **2021**, *47*, 8879–8887, https://doi.org/10.1016/j.ceramint.2020.12.009.
35. Ashokan, A.; Rajendran, V.; Sampath Kumar, T.S.; Jayaraman, G. Eggshell Derived Hydroxyapatite Microspheres for Chromatographic Applications by a Novel Dissolution - Precipitation Method. *Ceram. Int.* **2021**, *47*, 18575–18583, https://doi.org/10.1016/j.ceramint.2021.03.183.
36. Capitelli, F.; Dida, B.; Ventura, G.D.; Baldassarre, F.; Capelli, D.; Senesi, G.S.; Mele, A.; Siliqi, D. Functional Nano-Hydroxyapatite for Applications in Conservation of Stony Monuments of Cultural Heritage. *Proceedings* **2021**, *62*, 11, https://doi.org/10.3390/proceedings2020062011.
37. Hassani, A.; Khoshfetrat, A.B.; Rahbarghazi, R.; Sakai, S. Collagen and Nano-Hydroxyapatite Interactions in Alginate-Based Microcapsule Provide an Appropriate Osteogenic Microenvironment for Modular Bone Tissue Formation. *Carbohydr. Polym.* **2022**, *277*, 118807, https://doi.org/10.1016/j.carbpol.2021.118807.
38. Hou, H.; Zhou, R.; Wu, P.; Wu, L. Removal of Congo Red Dye from Aqueous Solution with Hydroxyapatite/Chitosan Composite. *Chem. Eng. J.* **2012**, *211–212*, 336–342, https://doi.org/10.1016/j.cej.2012.09.100.
39. Aliabadi, M.; Irani, M.; Ismaeili, J.; Najafzadeh, S. Design and Evaluation of Chitosan/Hydroxyapatite Composite Nanofiber Membrane for the Removal of Heavy Metal Ions from Aqueous Solution. *J. Taiwan Inst. Chem. Eng.* **2014**, *45*, 518–526, https://doi.org/10.1016/j.jtice.2013.04.016.
40. Ozola-Davidane, R.; Burlakovs, J.; Tamm, T.; Zeltkalne, S.; Krauklis, A.E.; Klavins, M. Bentonite-Ionic Liquid Composites for Congo Red Removal from Aqueous Solutions. *J. Mol. Liq.* **2021**, *337*, 116373, https://doi.org/10.1016/j.molliq.2021.116373.
41. Jiang, Q.; Zhao, C.; Han, Z.; Yang, G.; Qu, N.; Sun, L.; Li, W.; Wang, M.; Cheng, Z. Amino-Functionalized Polyacrylonitrile/Bentonite Composite Membranes for Effective Decontamination of Pb2+ and Congo Red. *Sep. Purif. Technol.* **2022**, *287*, 120606, https://doi.org/10.1016/j.seppur.2022.120606.
42. Karaman, C.; Karaman, O.; Show, P.-L.; Karimi-Maleh, H.; Zare, N. Congo Red Dye Removal from Aqueous Environment by Cationic Surfactant Modified-Biomass Derived Carbon: Equilibrium, Kinetic, and Thermodynamic Modeling, and Forecasting via Artificial Neural Network Approach. *Chemosphere* **2022**, *290*, 133346, https://doi.org/10.1016/j.chemosphere.2021.133346.
43. Sricharoen, P.; Chanthai, S.; Lamaiphan, N.; Sakaew, C.; Limchoowong, N.; Nuengmatcha, P.; Oh, W.-C. Sono-Synthesized Fe_3O_4–GO–NH_2 Nanocomposite for Highly Efficient Ultrasound-Assisted Magnetic Dispersive Solid-Phase Microextraction of Hazardous Dye Congo Red from Water Samples. *J. Korean Ceram. Soc.* **2021**, *58*, 201–211, https://doi.org/10.1007/s43207-020-00089-y.